METRICA
METRology Institutional CAtalog

ISTITUTO NAZIONALE DI RICERCA METROLOGICA
Repository Istituzionale

Designer SiO2 Metasurfaces for Efficient Passive Radiative Cooling

Original
Designer SiO2 Metasurfaces for Efficient Passive Radiative Cooling / Ding, Z.m., Li, H.l., Li, X., Fan, X.y., Jaramillo-Fernandez, J., Pattelli, L., Zhao, J.p., Niu, S.c., Li, Y., Xu, H.b.. - In: ADVANCED MATERIALS INTERFACES. - ISSN 2196-7350. - 11:3(2023). [10.1002/admi.202300603]

Availability:
This version is available at: 11696/78539 since: 2024-01-23T16:08:43Z

Publisher:
WILEY

Published
DOI:10.1002/admi.202300603

Terms of use:

This article is made available under terms and conditions as specified in the corresponding bibliographic description in the repository

Publisher copyright

(Article begins on next page)

09 November 2026

ADVANCED MATERIALS INTERFACES
Open Access
www.advmatinterfaces.de

Check for updates

Designer SiO_2 Metasurfaces for Efficient Passive Radiative Cooling

Zhenmin Ding, Honglin Li, Xin Li, Xueying Fan, Juliana Jaramillo-Fernandez, Lorenzo Pattelli, Jiupeng Zhao, Shichao Niu, Yao Li,* and Hongbo Xu**

In recent years, an increasing number of passive radiative cooling materials are proposed in the literature, with several examples relying on the use of silica (SiO_2) due to its unique stability, non-toxicity, and availability. Nonetheless, due to its bulk phonon-polariton band, SiO_2 presents a marked reflection peak within the atmospheric transparency window (8-13 µm), leading to an emissivity decrease that poses a challenge to fulfilling the criteria for sub-ambient passive radiative cooling. Thus, the latest developments in this field are devoted to the design of engineered SiO_2 photonic structures, to increase the cooling potential of bulk SiO_2 radiative coolers. This review seeks to identify the most effective photonic design and fabrication strategies for SiO_2 radiative emitters by evaluating their cooling efficacy, as well as their scalability, providing an in-depth analysis of the fundamental principles, structural models, and results (both numerical and experimental) of various types of SiO_2 radiative coolers.

1. Introduction

Passive Radiative Cooling (PRC) is a spontaneous effect by which an object can dissipate its thermal energy to outer space through the atmospheric transparency windows (8–13 µm), possibly reaching a sub-ambient temperature.[1–3] This effect could not just help reduce our growing electricity needs for cooling but also help curb global warming and greenhouse gas emissions. When combined with high solar reflectivity, a net radiative heat loss can be achieved even under direct sunlight.[4–8] For these reasons, radiative coolers have gained popularity due to their ability to act as heat dissipation channels in conjunction with existing conduction and convection processes.[9–11] Furthermore, their scalability and cost-effectiveness in thin-film form hold promise for their application in photovoltaic cells and space-cooling infrastructures.[12–15]

The field of nanotechnology and metamaterials witnessed rapid progress, resulting in the development of several photonic designs with spectral selectivity for diverse radiative coolers.[16] The key to achieving daytime cooling lies in reducing solar absorption and enhancing mid-infrared emission. To attain a high level of solar reflectance, it is customary to employ reflective metallic or highly scattering structures.[17–20] Silica (SiO_2) is frequently chosen as a constituent material owing to its vanishing absorption in the solar band and high emissivity in the mid-long-infrared band.[21–24] The use of SiO_2 in radiative cooling materials comes mainly in two forms: multilayer films and composite film fillers. For instance, Raman et al.[25] designed a metal-dielectric photonic multilayer endowed with selective emissivity in the mid-infrared band thanks to an alternating multilayer of HfO_2 and SiO_2 on a silicon wafer substrate. The resulting high emissivity in the atmospheric window (8–13 µm) was primarily due to the interference of the layer stack, demonstrating PRC

Z. Ding, H. Li, X. Li, X. Fan, J. Zhao, H. Xu
School of Chemistry and Chemical Engineering
Harbin Institute of Technology
Harbin 150001, P. R. China
E-mail: iamxhb@hit.edu.cn
J. Jaramillo-Fernandez
Departament de Maquines i Motors Termics
Universitat Politècnica de Catalunya
Diagonal 647, Barcelona 08028, Spain
The ORCID identification number(s) for the author(s) of this article can be found under https://doi.org/10.1002/admi.202300603

© 2023 The Authors. Advanced Materials Interfaces published by Wiley-VCH GmbH. This is an open access article under the terms of the Creative Commons Attribution License, which permits use, distribution and reproduction in any medium, provided the original work is properly cited.

DOI: 10.1002/admi.202300603

J. Jaramillo-Fernandez
Cooling Photonics S.L.
Carrer de Sant Joan de La Salle 42, Barcelona 08022, Spain
L. Pattelli
Istituto Nazionale di Ricerca Metrologica (INRiM)
Turin 10135, Italy
E-mail: pattelli@lens.unifi.it
L. Pattelli
European Laboratory for Non-linear Spectroscopy (LENS)
Sesto Fiorentino 50019, Italy
S. Niu
Key Laboratory of Bionic Engineering (Ministry of Education, China)
Jilin University
Changchun 130022, P. R. China
Y. Li
Center for Composite Materials and Structure
Harbin Institute of Technology
Harbin 150001, P. R. China
E-mail: yaoli@hit.edu.cn

21967350, 2024, 3, Downloaded from https://onlinelibrary.wiley.com/doi/10.1002/admi.202300603 by Istituto Nazionale Di Ricerca Metrologica, Wiley Online Library on [26/01/2024]. See the Terms and Conditions (https://onlinelibrary.wiley.com/terms-and-conditions) on Wiley Online Library for rules of use; OA articles are governed by the applicable Creative Commons License

under direct sunlight experimentally for the first time. A more scalable approach was successively proposed by Zhai et al.[26] who demonstrated efficient day- and night-time radiative cooling with an emitter made of randomized SiO_2 microspheres in a polymethylpentene film. This composite material exhibited an emissivity exceeding 0.93 across the atmospheric window, which was attributed to the phonon-polariton resonance of the SiO_2 microspheres at a wavelength of 9.7 µm.

Investigation into the use of SiO_2 to improve emissivity and cooling has been extensive, yet a comprehensive and up-to-date overview is still lacking. SiO_2 radiative coolers offer several advantages over recently proposed polymer-based radiative cooling materials,[27] starting with their extreme robustness against ultraviolet (UV) irradiation, which makes them usable also in the harsh conditions of space applications.[15] Similarly, SiO_2 offers excellent flame resistance compared to most polymeric radiative cooling materials, which is an important factor for many applications in the building sector.[28] Furthermore, SiO_2 is a naturally abundant, infinitely recyclable, and non-toxic material posing no health-related or environmental hazard, which stands in contrast to the growing concerns on fluorinated polymers such as polytetrafluoroethylene (PTFE) and polyvinylidene fluoride (PVDF) often proposed for radiative cooling applications,[29,30] or the risk of microplastics release in the environmental due to their wearing with prolonged exposure to weathering agents.[31] For these reasons, interest in PRC emitters that are made exclusively by SiO_2 on metalized reflective substrates is growing due to their broad availability, stability, and reproducibility, making them a promising candidate for several applications in harsh environments, as well as for the realization of standardized coolers. Pure SiO_2 radiative coolers can be classified into different types based on their surface microstructure models, namely flat layers, nedimensional (1D) gratings, two-dimensional (2D) patterns, and ordered and disordered microsphere layers. In this review article, we will expound on the state-of-the-art advancements concerning pure SiO_2 PRC devices. After a brief presentation of the fundamental principle of PRC, the diverse applications of SiO_2 emitters will be discussed (including but not limited to solar cell cooling). Finally, the current limitations and prospects of SiO_2 PRC devices will be presented.

2. Fundamentals of Radiative Sky Cooling

The principle of PRC is based on the conservation of energy. All sky-facing devices are affected by solar irradiance and downward thermal radiation from the atmosphere when they are exposed to a clear sky. At the same time, due to the temperature difference between the cooler and the surrounding environment, heat can be transferred between the two through conduction and convection. **Figure 1** shows the energy balance of the cooler surface. To achieve a net PRC effect, strict constraints must be met in the power balance equation. The net cooling power P_{net} can be expressed as:[32]

$$P_{net}(T) = P_{rad}(T) - P_{atm}(T_{atm}) - P_{solar} - P_{cond+conv} \quad (1)$$

Where T represents the surface temperature of the cooler and T_{atm} represents the ambient temperature. P_{rad} represents the outward heat radiation of the cooler surface, P_{solar} represents the radiation absorbed from the sun, P_{atm} represents the thermal radiation absorbed from the atmosphere, and $P_{cond+conv}$ represents the non-radiative heat transfer power between the cooler and the surrounding environment, namely conduction and convection.

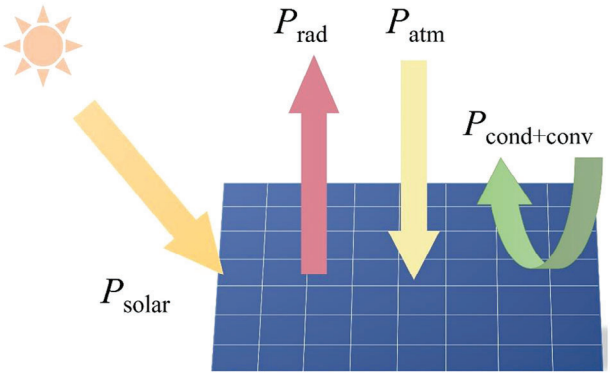


Figure 1. Main terms in the heat transfer energy balance for a sky-facing cooler surface.

P_{rad} represents the outward radiated power of the object, which refers to the total radiated power emitted from its surface per unit area at all wavelengths and in all directions, as expressed by the following formula:

$$P_{rad}(T) = A \int d\Omega \cos\theta \int_0^\infty d\lambda I_{BB}(T,\lambda)\,\varepsilon(\lambda,\theta) \quad (2)$$

Where A is the surface area of the cooler and $\int d\Omega = 2\pi \int_0^{\frac{\pi}{2}} d\theta \sin\theta$ is the hemispheric angle integral. $\epsilon(\lambda, \theta)$ is the emissivity of the radiator at wavelength λ, $I_{BB}(T,\lambda) = \frac{2hc^2}{\lambda^5}\frac{1}{e^{hc/(\lambda k_B T)}-1}$ is the blackbody radiation spectrum intensity at temperature T, with h, k_B and c as the Planck, Boltzmann and speed of light constants, respectively.

P_{atm} describes the fraction of the downwards radiation from the atmosphere that is absorbed by the radiative cooler, expressed as:

$$P_{atm}(T_{atm}) = A \int d\Omega \cos\theta \int_0^\infty d\lambda I_{BB}(T_{atm},\lambda)\,\varepsilon(\lambda,\theta)\,\varepsilon_{atm}(\lambda,\theta) \quad (3)$$

where $\epsilon_{atm}(\lambda,\theta) = 1 - \tau(\lambda)^{1/\cos\theta}$ is the atmospheric emissivity and $\tau(\lambda)$ is the atmospheric transmittance at zenith.

P_{solar} is the incident solar irradiation absorbed by the cooler:

$$P_{solar} = A \int_0^\infty d\lambda \varepsilon(\lambda,\theta_{solar}) I_{AM1.5}(\lambda) \quad (4)$$

where $I_{AM1.5}(\lambda)$ is the air mass (AM) 1.5 spectrum distribution of the solar radiation intensity varying with the wavelength, and θ_{solar} is the inclination of the sample surface toward the sun.

The non-radiative heat transfer power of $P_{cond+conv}$ can be described according to Newton's law:[33]

$$P_{cond+conv}(T,T_{atm}) = Ah_c(T_{atm} - T) \quad (5)$$

where h_c is the non-radiative heat transfer coefficient, which subsumes the conduction and convective heat transfer terms as $h_c = h_{cond} + h_{conv}$, and can take typical values between 0 and

© 2023 The Authors. Advanced Materials Interfaces published by Wiley-VCH GmbH

21967350, 2024, 3, Downloaded from https://onlinelibrary.wiley.com/doi/10.1002/admi.202300603 by Istituto Nazionale Di Ricerca Metrologica, Wiley Online Library on [26/01/2024]. See the Terms and Conditions (https://onlinelibrary.wiley.com/terms-and-conditions) on Wiley Online Library for rules of use; OA articles are governed by the applicable Creative Commons License

12 W m^{-2} K^{-1} depending on the level of thermal insulation of the emitter and local wind speed.

When the temperature of the cooler is equal or higher than the ambient temperature($T \geq T_{atm}$), there is a net positive power outflow, namely $P_{cooling} > 0$, in this case, the cooler can continuously radiate energy outward to reduce its own temperature. On the contrary, at $P_{cooling} = 0$, the temperature of the emitter stabilizes, reaching the stagnation temperature, which is generally used to characterize the below-ambient cooling performance of the surface. According to equation (1), the ideal conditions to enhance the net cooling power require to maximize P_{rad} and minimize P_{solar}, P_{atm}, and $P_{cond+conv}$. Hence, the cooler needs to exhibit vanishing absorption in the solar wavelength range as a primary condition to minimize P_{solar}. Second, the cooler needs to have a high level of emissivity in the infrared, especially in the atmospheric window band, to maximize P_{rad}. It is also necessary to minimize the downward atmospheric radiation (P_{atm}) absorbed by the radiator. In practice, to achieve meaningful daytime radiative cooling, the cooler must reject more than 94% of the solar energy, allowing it to be applied to areas with different weather conditions. At the same time, the test device needs to be properly insulated to minimize the non-radiative heat transfer coefficient h_c and thus minimize $P_{cond+conv}$.

The cooling performance of a PRC device depends critically on the mean solar reflection ($\bar{R}_{solar}$):[34]

$$\bar{R}_{solar} = \frac{\int_{0.25\mu m}^{2.5\mu m} I_{solar}(\lambda)\, R(\lambda)\, d\lambda}{\int_{0.25\mu m}^{2.5\mu m} I_{solar}(\lambda)\, d\lambda} \quad (6)$$

where $R(\lambda)$ is the material reflectivity, and $I_{solar}(\lambda)$ is the normalized American Society for Testing and Materials (ASTM) G-173 Global solar intensity spectrum.

At the same time, a strong thermal emissivity in the infrared range is also important for a sustained radiative cooling. The emissivity contribution at the atmospheric window wavelengths ($\epsilon_{8-13\mu}$) can be calculated as:

$$\varepsilon_{8-13\mu m} = \frac{\int_{8\mu m}^{13\mu m} I_{BB}(T,\lambda)\, \varepsilon(T,\lambda)\, d\lambda}{\int_{8\mu m}^{13\mu m} I_{BB}(T,\lambda)\, d\lambda} \quad (7)$$

where $I_{BB}(T,\lambda)$ is the spectral intensity of blackbody radiation and $\epsilon(T, \lambda)$ is the spectral emissivity of the cooler. According to Kirchhoff's law, for any object in thermal equilibrium, spectral absorption and spectral emissivity must be equal. Therefore, emissivity can be defined as:[35]

$$\varepsilon = 1 - R - T \quad (8)$$

where T is transmittance and R is the reflectance in IR spectroscopy.

The typical reflectance of silver-plated SiO_2 in the solar band (0.25–2.5 µm) is ≈95%.[36,37] The average emissivity of a bulk SiO_2 sample in the atmospheric window (8–13 µm), however, is only ≈0.75. By changing the emissivity of the bulk SiO_2 surface, the cooling capacity of the emitter composed of this SiO_2 can be improved. Assuming a 25 °C ambient temperature, with non-radiative heat exchange (12 W m^{-2} K^{-1}) with the environment and absorption of 0.05 in the solar band, the radiative power of

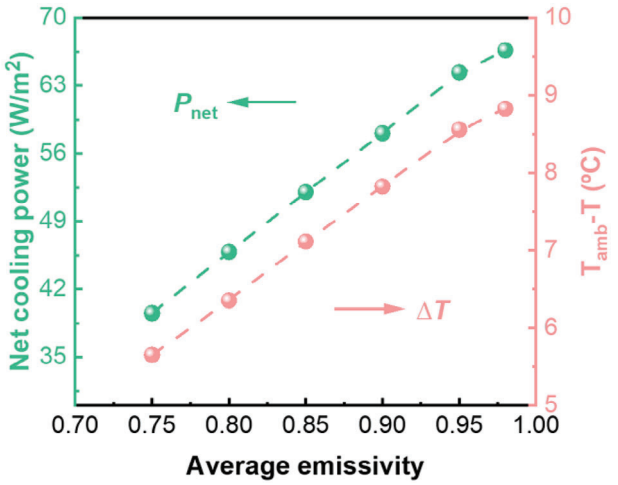


Figure 2. Net theoretical cooling flux P_{net} (calculated at $T = T_{amb}$) and temperature difference $\Delta T = T_{amb} - T$ (calculated at $P_{net} = 0$) for different SiO_2 emitters as a function of sample average emissivity (T represents the surface temperature of the SiO_2 emitters, T_{amb} = 25 °C, h_{cc} = 12 W m^{-2} K^{-1}).

SiO_2 emitter and the atmosphere in the 8–13 µm band can be calculated using Equations 2 and 3, respectively. Combined with Equation 1, the overall net cooling power obtained shows a direct proportionality with infrared emissivity. By considering a set of representative values of the average emissivity in the atmospheric transparency window ranging from the bulk case to the highest value reported obtained experimentally in the literature for a SiO_2 emitter (ϵ_{avg} = 0.98[38–40]), we see that the expected temperature drop can potentially increase from 5.3 °C to 8.8 °C, with a corresponding net cooling power enhancement of more than 27 W m^{-2} (**Figure 2** and **Table 1**). How to achieve such high average emissivity values in practice for SiO_2 emitters and hence take full advantage of this additional net cooling power will be the main subject of this review.

3. Development of Advanced SiO_2 Radiative Cooling Devices

3.1. Basic properties of SiO_2-Based Materials

Silicon dioxide (SiO_2), also commonly referred to as silica, is an abundant naturally occurring compound. Owing to its

Table 1. Calculated radiative and cooling capacities for different SiO_2 emitters.

$\epsilon_{avg(8\text{-}13\ \mu m)}$	P_{rad} [W m^{-2}]	P_{atm} [W m^{-2}]	P_{solar} [W m^{-2}]	P_{net} [W m^{-2}]	ΔT [°C]
0.75	108.0	23.8	44.7	39.5	5.3
0.80	115.4	24.9	44.7	45.8	6.1
0.85	122.4	25.7	44.7	52.0	6.9
0.90	129.5	26.7	44.7	58.1	7.7
0.95	136.8	27.8	44.7	64.4	8.5
0.98	141.2	29.8	44.7	66.7	8.8

© 2023 The Authors. Advanced Materials Interfaces published by Wiley-VCH GmbH

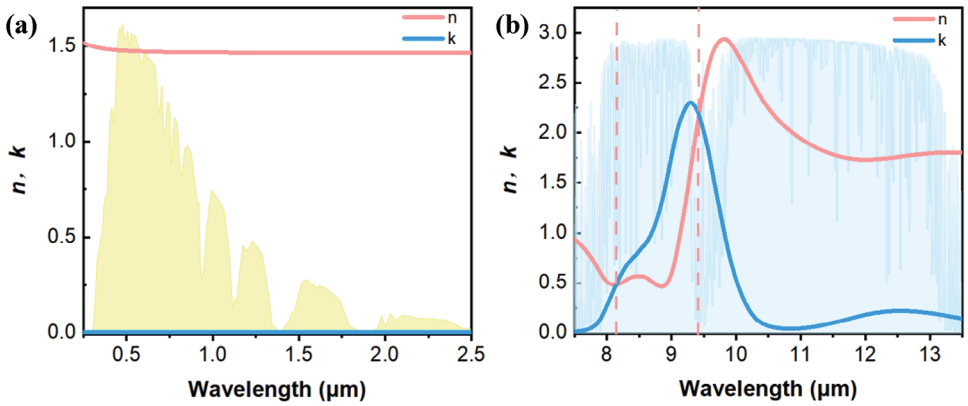


Figure 3. Optical refractive index (n) and absorption coefficients (k) of bulk SiO_2 in different bands[49]: a) solar spectral band (0.25–2.5 μm); b) atmospheric window band (8–13 μm). The region between two red dashed lines is the reststrahlen band.

remarkable physical and chemical properties, SiO_2 is a versatile material that finds applications in a wide range of industries and research fields such as electronics, photonics, precision optics glass manufacturing, and aerospace, to name a few. Furthermore, due to its excellent stability, hardness, environmental friendliness, and optical transparency across the solar spectrum, SiO_2 is well-suited for outdoor applications. For example, it is often used as a component in solar reflective paints and protective coatings and is the main component of photovoltaic glass covers and windows.[41] As such, SiO_2 has also recently emerged as a suitable material for daytime sub-ambient radiative cooling.

In its purest form, usually denoted as fused silica, this material features high transmittance across the solar spectrum and down to the ultraviolet, exhibiting a sharp UV cutoff resulting from strong absorption bands below 0.2 μm caused by the interaction of light with electrons of Si-O bonds, impurities and the presence of OH groups. Its remarkable transmittance is owed to its absorption coefficient, which effectively vanishes between 0.2 and 4.0 μm. For longer wavelengths, silica is mainly opaque, but its extinction coefficient has strong peaks at 9–9.5 μm due to Si-O-Si resonance modes of vibration, also known as its bulk phonon–polariton resonances.[42,43] This causes a strong impedance mismatch at the SiO_2-air interface, which in turn leads to increased reflectance in the mid-infrared band.[44] Electromagnetic radiation with frequencies in that range cannot propagate through the material, causing a metallic-like reflectance bandgap (Reststrahlen) which is detrimental for radiative cooling applications.[45–47] Moreover, as shown in **Figure 3a**, bulk SiO_2 exhibits an extinction coefficient close to zero in the solar spectral band (0.25–2.5 μm), indicating its vanishing absorption in this band. In the atmospheric transparency window (8–13 μm), on the other hand, bulk SiO_2 has a high reflectance near 9 μm, due to the strong modulation of its permittivity around this wavelength. This is evidenced by the intersection of the refractive index (n) and extinction coefficient (k) of bulk silica at 8.1 and 9.3 μm, respectively, which represent the longitudinal (LO) and transverse (TO) optical phonon frequencies (Figure 3b).[43] In this range (8.1–9.3 μm), the real part of the dielectric constant becomes negative, resulting in weakened propagation and increased reflectivity, thus creating a reststrahlen band. If the reflectivity of SiO_2 in the reststrahlen band can be reduced without altering its composition and intrinsic structure, then pure SiO_2 can become a prominent material for a range of mid-infrared applications. To this end, surface patterning is a promising strategy to address the wavevector mismatch at the air-SiO_2 interface and allow the coupling of radiation to the surface phonon polaritons, by creating a smoother transition between the two materials.[48]

The relation between reflectivity and the impedance mismatch at the interface between two media is a general concept, valid for all types of waves. In the electromagnetic case, the complex-valued impedance is expressed in Ohms and links the amplitude of the transverse electric and magnetic fields depending on the electric permittivity ϵ and magnetic permeability μ of the medium via the relation:

$$Z = \frac{E}{H} = \left(\frac{\mu}{\epsilon}\right)^{1/2} \tag{9}$$

Considering for simplicity the case of normal incidence, the reflectivity at the interface between two media (e.g., air and SiO_2) can be expressed in terms of the difference of their wave impedance values as:[50]

$$R = \left|\frac{Z_2 - Z_1}{Z_2 + Z_1}\right|^2 \tag{10}$$

which can be easily generalized to different incidence angles and polarizations. For non-magnetic media, the complex refractive index of a material can be seen as the ratio between the impedance of vacuum and the medium's impedance, which allows to recover the familiar Fresnel reflection coefficients.

Although the overall optical properties of SiO_2 remain consistent among various forms of crystalline silica and amorphous glasses derived from the SiO_2 compound, the specific values of the refractive index and extinction coefficient can vary appreciably based on factors as the degree of crystallinity, the manufacturing process and the presence of impurities like inclusions and minerals. For example, soda-lime glass and borosilicate glass are two common types of glass that are made with SiO_2 as their principal component, but they differ in their composition of added minerals and impurities, which results in variations of the optical properties. While fused silica is highly reflective in the atmospheric window region (≈70%), the added impurities in soda

© 2023 The Authors. Advanced Materials Interfaces published by Wiley-VCH GmbH

21967350, 2024, 3, Downloaded from https://onlinelibrary.wiley.com/doi/10.1002/admi.202300603 by Istituto Nazionale Di Ricerca Metrologica, Wiley Online Library on [26/01/2024]. See the Terms and Conditions (https://onlinelibrary.wiley.com/terms-and-conditions) on Wiley Online Library for rules of use; OA articles are governed by the applicable Creative Commons License

Table 2. Summary of different types of SiO_2 radiative coolers reported in recent years.

Structure	Study type	Temperature drop [°C]	Average emissivity	Cooling Power [W m^{-2}]	Reference (year)
Flat film	Experimental	–	–	–	Granqvist et al. (1981)[54]
	Experimental	7	–	–	Zhang et al. (2019)[55]
	Experimental	–	–	–	Ishii et al. (2020)[56]
	Experimental	5.9	0.85	–	Zhao et al. (2019)[36]
Silica fibers	Numerical	–	–	178	Yalçın R A et al. (2020)[57]
	Experimental	6.0	0.90	112	Tsai et al. (2023)[28]
1D gratings	Numerical	31.4	–	–	Zhu et al. (2013)[58]
	Numerical	–	–	114	Blandre et al. (2020)[59]
	Numerical	–	> 0.90	98	Liu et al. (2021)[60]
	Experimental	3.6	0.91	–	Zhao et al. (2022)[61]
2D micropatterns	Experimental	13	–	–	Zhu et al. (2015)[62]
	Experimental	2	–	600	Long et al. (2019)[63]
	Numerical	9	≈1.0	121	Li et al. (2022)[64]
	Experimental	7	0.952	–	Pinto et al. (2023)[52]
	Numerical	17.6	≈1.0	–	Zhu et al. (2014)[45]
	Experimental	–	> 0.96	–	Lu et al. (2017)[65]
	Experimental	9.2	> 0.98	–	Fathabadi et al. (2021)[38]
	Experimental	3	0.977	–	Akerboom et al. (2022)[39]
	Experimental	7.1	0.95	143	Ding et al. (2022)[37]
	Experimental	–	0.947	–	Arrés Chillón et al. (2022)[66]
Microspheres	Experimental	–	> 0.94	–	Atiganyanun et al. (2018)[67]
	Experimental	≈6.9	–	–	Fan et al. (2020)[68]
	Numerical	73	–	–	Whitworth et al. (2021)[53]
	Experimental	19	>0.98	350	Fernandez et al. (2019)[40]
	Experimental	5	0.946	–	Lin et al. (2022)[69]
	Numerical	–	0.916	80	Chen et al. (2021)[70]

lime glass reduce the reflectance in the reststrahlen band resulting in a relatively lower reflectance in the desired region (≈30%), compared to that of pure fused-SiO_2. Various photonic techniques also have been utilized to enhance the surface structure of SiO_2 to improve its spectral properties of the reststrahlen band through the generation of Mie scattering effects or the excitation of phonon polariton resonances between the SiO_2 microstructures. Some of these fabrication techniques have been applied to the case of borosilicate glasses, soda lime glasses, and silicon carbide, resulting in improved spectra of the reststrahlen bands of these materials.[51–53]

In the past decade, however, the advancement of microfabrication and patterning methods has led to the rapid development of SiO_2 radiative cooling materials with various photonic structures. **Table 2** summarizes key indicators of recent SiO_2 coolers used for both above-ambient and sub-ambient cooling applications, which can be broadly classified into flat films, 1D gratings, 2D micropatterns, and microspheres.

3.2. SiO_2 Flat Films

The selective emissivity of SiO thin films within the atmospheric window was first highlighted in 1981, despite the fact that SiO film does not exhibit sustained reflectivity across its whole wavelength range (see **Figure 4a**).[54] A high reflectance is observed ≈9 µm, which is commonly known as the reflective reststrahlen band in this particular spectral range. More recently, Zhang and co-workers[55] reported that a pure SiO_2 film can provide an average nighttime cooling capacity of 7 °C, as depicted in Figure 4b. Additionally, Ishii et al.[56] developed a SiO_2 radiative cooler with an aluminum film that can continuously cool one side of a thermoelectric module during day and night, hence generating an uninterrupted voltage. Zhao and co-workers[36] also fabricated a radiative cooling film using pure SiO_2, revealing a marked decrease in the emissivity of this material in the atmospheric window band (Figure 4c), associated with the impedance mismatch ≈9 µm at the flat SiO_2-air interface.

3.3. 1D Gratings

Creating a pattern on the surface of pure SiO_2 is an effective method to increase its emissivity in the 8–13 µm range. Zhu et al.[58] proposed a SiO_2 emitter featuring a 1D grating microstructure, which has been utilized for radiative cooling of outdoor electronic devices. This grating structure exhibits a periodicity of 7 µm and a height of 10 µm, as illustrated in **Figure 5a**,

© 2023 The Authors. Advanced Materials Interfaces published by Wiley-VCH GmbH

21967350, 2024, 3, Downloaded from https://onlinelibrary.wiley.com/doi/10.1002/admi.202300603 by Istituto Nazionale Di Ricerca Metrologica, Wiley Online Library on [26/01/2024]. See the Terms and Conditions (https://onlinelibrary.wiley.com/terms-and-conditions) on Wiley Online Library for rules of use; OA articles are governed by the applicable Creative Commons License

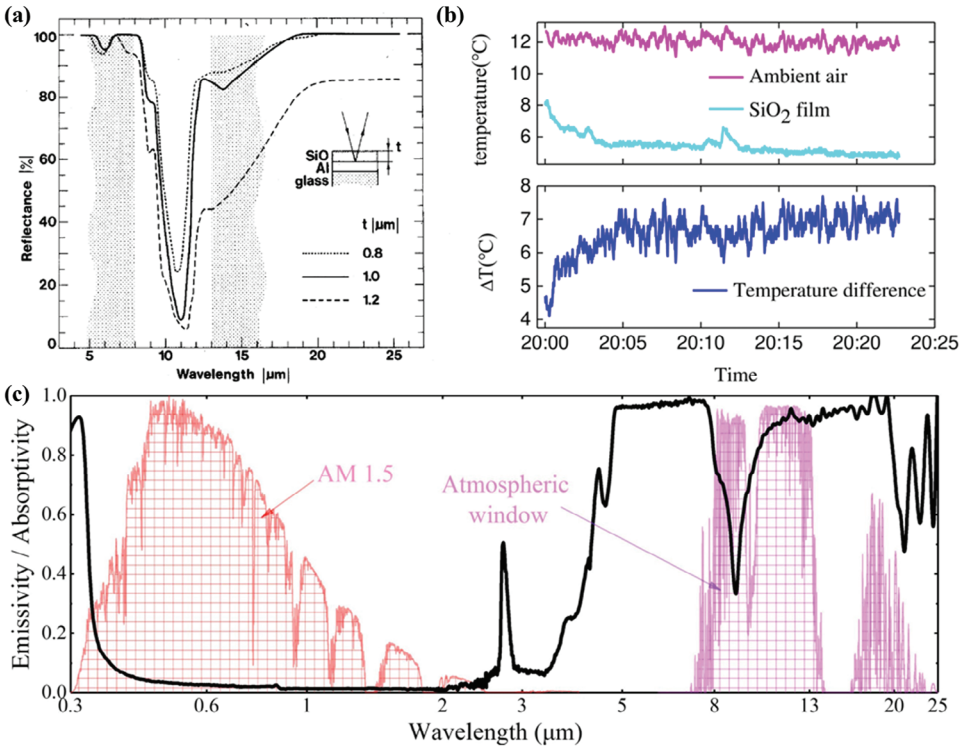


Figure 4. Flat film thermal emitter design. a) The spectral reflectance of SiO films deposited onto aluminized glass substrates. Reproduced with permission.[54] Copyright 1981, AIP Publishing. b) Temperature change of SiO_2 film. Reproduced with permission.[55] Copyright 2019, Proceedings-of-SPIE. Measured emissivity/absorptivity of a SiO_2 mirror emitter. Reproduced with permission.[36] Copyright 2019, Elsevier.

endowing the structure with a significantly enhanced emissivity compared to the case of pure SiO_2 (Figure 5b). Liu et al.[60] investigated systematically the impact of 1D gratings and 2D micropillars on the emissivity of bulk SiO_2 in the 8–13 μm band. The models constructed for this study are presented in Figure 5c,e. The results, as illustrated in Figure 5d,f, revealed that the 2D micropillar provided a higher emissivity enhancement, with predicted net cooling powers of 98 and 105 W m^{-2}, respectively. Blandre et al.[59] also reported similar results from comparing different one- and 2D Ag-SiO_2 structured grating radiative coolers.

While theoretical simulations are undoubtedly useful, however, the practical feasibility of many numerically designed SiO_2 radiative cooling devices proposed in the literature is heavily dependent on the awareness of the technical constraints for their experimental fabrication. Zhao et al.[61] utilized photolithography and inductively coupled plasma etching to fabricate a 1D grating structure on the surface of SiO_2. The resulting surface, depicted in Figure 5g, has a structured period of 7 μm, a grating duty cycle of 0.2, and an etching depth of 10 μm. The corresponding IR emissivity spectra, shown in Figure 5h, indicate an increase in average emissivity from 0.81 to 0.91 due to the design of the micro-grating partially overcoming the impedance mismatch at the air-SiO_2 interface. These results show that 1D gratings represent a viable strategy to increase the infrared emissivity of bulk SiO_2. This is due to the fact that the grating can enhance the coupling between the incident light and the surface of the SiO_2, thus overcoming the impedance mismatch at the air-SiO_2 interface. Furthermore, the 1D grating microstructures have a large size (average period > 7 μm) and a low extinction coefficient of SiO_2 in the solar band ($k \approx 0$, Figure 3a), which do not affect the spectral response at these wavelengths.

3.4. 2D micropatterns

Compared to 1D gratings, 2D micropatterns tend to show greater emissivity enhancement. Targeting the construction of 2D micropatterns on SiO_2 surfaces, Ray et al.[71] first reviewed the prospects for the application of glass optical super-surfaces, confirming that these etched surfaces are mechanically durable and scalable, and demonstrating the feasibility of directional etching techniques such as reactive ion beam etching (RIBE) and reactive ion etching (RIE) for the processing of 2D glass micropillar arrays. Thus, based on prior evidence from numerical simulations, significant efforts have been made toward the development of 2D micropillars to further enhance the thermal emissivity of SiO_2. **Figure 6**a depicts one of the early examples of a 2D array of micropillars with a diameter of 6 μm and a period of 10 μm obtained via photolithography and ion beam etching in 2015.[62] The corresponding emissivity at 8–13 μm was significantly increased compared to the flat case, as demonstrated in Figure 6b. Upon application of the SiO_2 cooler onto a silicon absorber, a remarkable temperature decrease of up to 13 °C was practically demonstrated, which holds significant practical importance for the efficiency of solar cells. In a similar vein, Long and co-workers[63] fabricated a 2D grating featuring a diameter of 5 μm and a period

© 2023 The Authors. Advanced Materials Interfaces published by Wiley-VCH GmbH

21967350, 2024, 3, Downloaded from https://onlinelibrary.wiley.com/doi/10.1002/admi.202300603 by Istituto Nazionale Di Ricerca Metrologica, Wiley Online Library on [26/01/2024]. See the Terms and Conditions (https://onlinelibrary.wiley.com/terms-and-conditions) on Wiley Online Library for rules of use; OA articles are governed by the applicable Creative Commons License

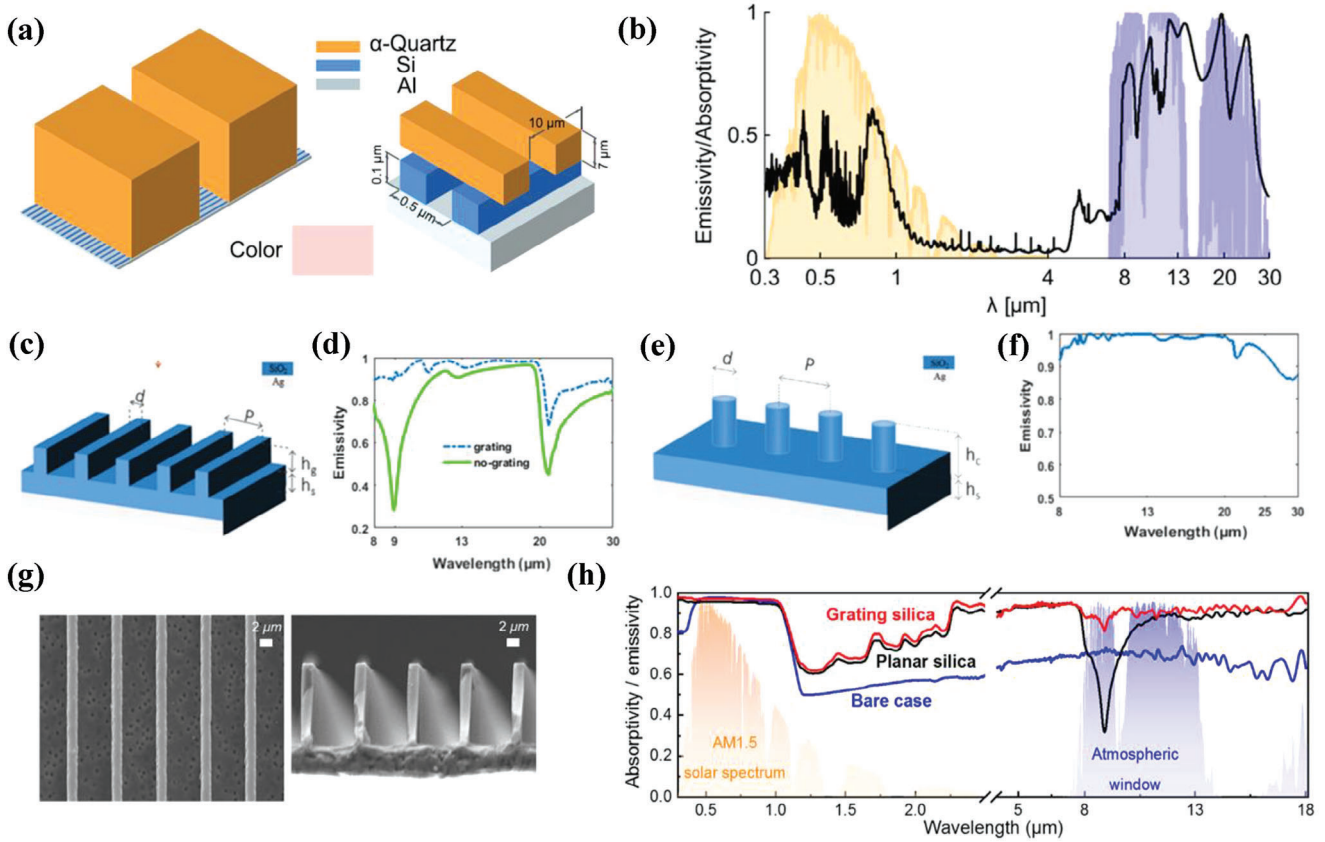


Figure 5. 1D gratings thermal emitter design. a) Schematic of the modified structure, with quartz bar array on top of the silicon nanowires. b) Emissivity/absorptivity spectrum of the modified structure. Reproduced with permission.[58] Copyright 2013, AIP Publishing. c) Structure of a SiO_2 grating with a period (P) of 12 μm, a ridge width of 2 μm, a SiO_2 layer thickness (h_s) of 100 μm, and a grating height (h_g) of 18 μm. d) The emissivity of the suggested configuration, with or without the grating, in the 8–30 μm wavelength range. e) Proposed grating with a period of 12 μm made of cylinders with a diameter of 4 μm and a height of 30 μm. f) Corresponding emissivity in the 8–30 μm wavelength range. Reproduced with permission.[60] Copyright 2021 by the authors. Licensee MDPI, Basel, Switzerland. g) Top-view and cross section view scanning electron microscope (SEM) images of SiO_2 grating. h) Measured solar absorptivity/emissivity of the bare cell, the cell with planar silica, and the cell with SiO_2 grating. Reproduced with permission.[61] Copyright 2022, Elsevier.

exceeding 10 μm, as depicted in Figure 6c–e. The resulting emissivity was also enhanced to exceed 0.9 (8–13 μm), as illustrated in Figure 6f. Li et al.[64] sought to further explore the intrinsic mechanism behind the emissivity enhancement of 2D micropillars. To achieve this, they simulated an array of truncated microcones on a silver-plated SiO_2 surface (Figure 6g), reaching almost unity emissivity within the 8–13 μm band for a truncated microcone height of 20 μm (Figure 6h). Pinto et al.[52] utilized microstructure processing techniques on glass cover materials to create periodic 2D cylindrical arrays, which drastically decreased the reflectivity at 9.5 μm (Figure 6i), consequently increasing the average emissivity of flat glass from 83% to 95% in the 8–13 μm range. This can be beneficial for photovoltaic (PV) systems, as it can enhance their efficiency and lifetime. This effect can be attributed to the gradient refractive index generated by the conical SiO_2 structure, the local phonon polariton resonance between the microcones, as well as the periodic lattice diffracting this excitation to the far field.

A special class of 2D grating-like structures, i.e., arrays of pyramidal structures, was also proposed in 2014 by Zhu and coworkers,[45] demonstrating near-unity infrared emissivity across the atmospheric window range (Figure 6j). In 2017, Lu and coworkers[65] utilized imprinting techniques to realize disordered pyramidal array structures, achieving an IR emissivity of ≈0.96 (Figure 6k). This value was further improved in 2021 by Fathabadi and co-workers[38] who demonstrated another disordered pyramidal array pattern with an emissivity close to 0.98 (Figure 6l).

Nonetheless, even though the microstructured SiO_2 samples exhibit a considerably greater emissivity, their patterning depth exceeding 5 μm and large periodic structure size surpassing 3 μm result in extreme fabrication costs and difficulties for their etching Hence, achieving comparable enhancements using smaller microstructured patterns could improve compatibility and expand the range of applications for microstructured SiO_2 radiative cooling materials.

Microstructures of small diameter and period are also advantageous as they decrease the risk of damage during processing and provide excellent device compatibility and structural stability. For these reasons, starting in 2022, there was a gradual shift towards developing small, microstructured SiO_2 arrays that could be more effectively integrated into various devices, including solar cells. Akerboom et al.[39] proposed a hexagonal array of pillars

© 2023 The Authors. Advanced Materials Interfaces published by Wiley-VCH GmbH

21967350, 2024, 3, Downloaded from https://onlinelibrary.wiley.com/doi/10.1002/admi.202300603 by Istituto Nazionale Di Ricerca Metrologica, Wiley Online Library on [26/01/2024]. See the Terms and Conditions (https://onlinelibrary.wiley.com/terms-and-conditions) on Wiley Online Library for rules of use; OA articles are governed by the applicable Creative Commons License

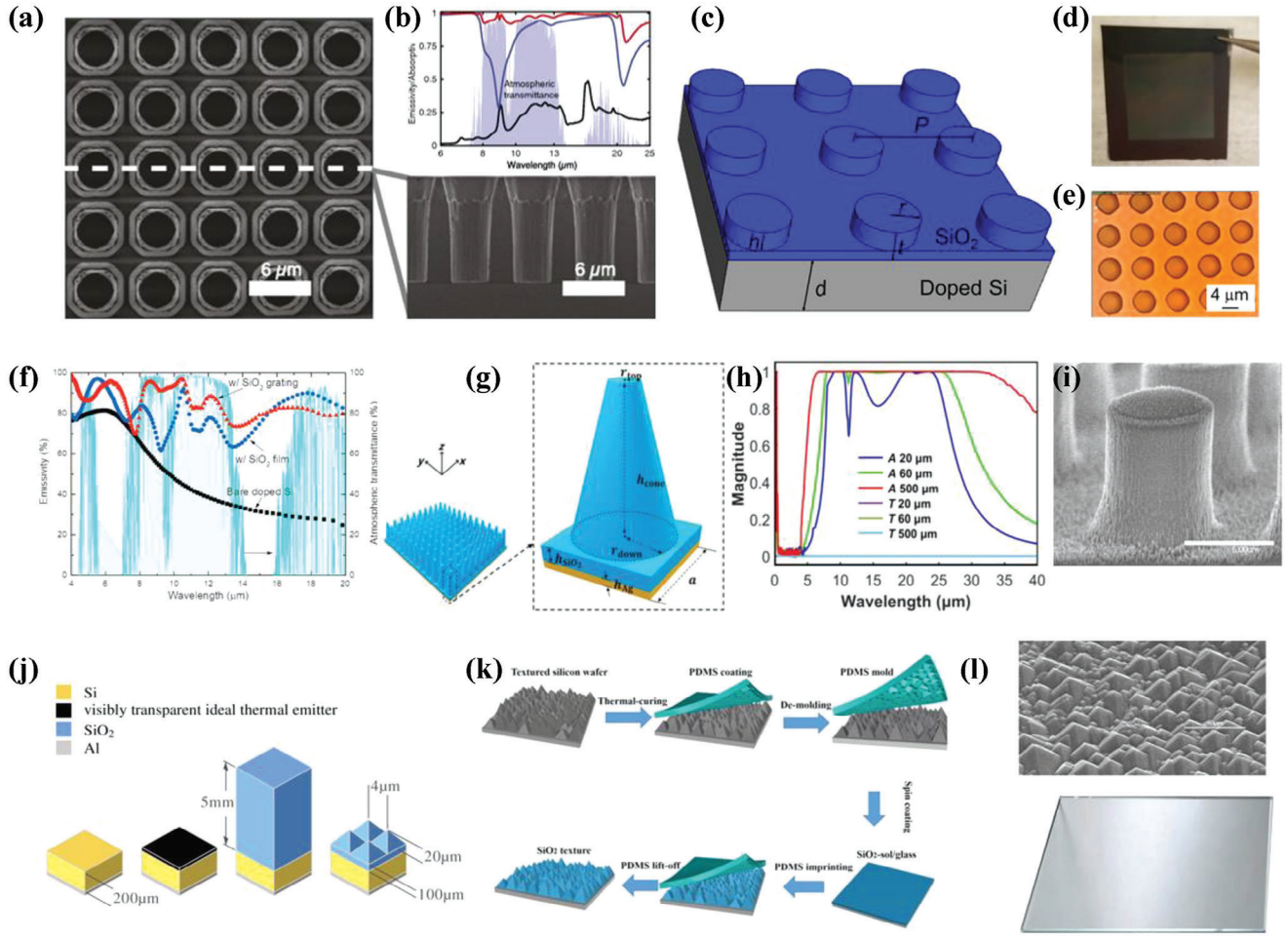


Figure 6. 2D micropillars/pyramidal micropillars thermal emitter design. a) Normal-view and side-view SEM images of the 2D SiO_2 photonic crystal structure with a periodicity of 6 μm made by etching 10-μm deep air holes into a 500-μm-thick double-side-polished fused SiO_2 wafer. b) The emissivity of solar absorbers at 10° angle of incidence over mid-infrared wavelengths. Reproduced with permission.[62] Copyright 2015, National Academy of Sciences. c) Schematic of SiO_2 grating atop doped Si layers. d) Photo of gratings on a Si wafer piece. e) Microscope image of the cylinder gratings. f) Thermal radiation spectrum with a wavelength from 4 to 20 μm. Reproduced with permission.[63] Copyright 2019, Elsevier. g) 3D geometry of the truncated microcone cooler for the sub-ambient daytime cooling in buildings. h) Absorptivity spectra of the designed cooler in 0.3-40 μm at different height values. Reproduced with permission.[64] Copyright 2022, Elsevier. i) Scanning electron microscope image of the microstructures. Reproduced with permission.[52] Copyright 2023, Wiley-VCH. j) 3D crystalline silicon solar cell structures. Reproduced with permission.[45] Copyright 2014, OSA Publishing. k) Schematic illustration of the photolithography-free preparation of sol–gel imprinted texture glass. Reproduced with permission.[65] Copyright 2017, Wiley-VCH. l) SEM photograph of the nanoscale pyramidal structure imprinted on the glass's surface and photograph of the fabricated glass with nano pyramidal coating. Reproduced with permission.[38] Copyright 2021, IEEE Electron Devices Society.

with a diameter of 3.65 μm and a structure height of 2.20 μm (**Figure** 7a). This structure increased the average emissivity of the pure SiO_2 sample in the 7.5-16 μm band from 84.3% to 97.7%, without reducing visible transmission (Figure 7b). This outcome was primarily attributed to the anti-reflective function of the multipole Mie resonance in the cylinders within the infrared spectrum, which ultimately led to an increase in the infrared emissivity. Ding and co-workers[37] fabricated a disordered array of truncated microcones on a SiO_2 surface, with a structural height of 2 μm and an average positional correlation of ≈1.1 μm (Figure 7c), leading to an average emissivity in the 8–13 μm band from 0.79 to ≈0.95 (Figure 7d). Arrés Chillón et al.[66] have developed a method for constructing dense arrays of small pillars on the surface of SiO_2. These pillars have an average diameter of ≈172 nm at the top and 286 nm at the bottom, with an average distance of 410 nm and a height of 1.25 μm (Figure 7e). The coupling between light and the surface phonon polariton (SPhP) of the SiO_2 in the nanopillar gap enhances the surface's infrared (IR) emissivity in the reststrahlen band (Figure 7f,g). This scalable lithography-free nanostructure approach reduces scattering (haze) from the glass by adding a thin polymer coating, which further extends the application of SiO_2 radiative coolers with small structured array surfaces, even though mechanical stability issues represents still a concern for structures with such high aspect ratios.[72]

One final consideration regarding 2D patterns in general, when compared to 1D structures, is that the spectral response of the former exhibits a much weaker polarization dependence,

© 2023 The Authors. Advanced Materials Interfaces published by Wiley-VCH GmbH

21967350, 2024, 3, Downloaded from https://onlinelibrary.wiley.com/doi/10.1002/admi.202300603 by Istituto Nazionale Di Ricerca Metrologica, Wiley Online Library on [26/01/2024]. See the Terms and Conditions (https://onlinelibrary.wiley.com/terms-and-conditions) on Wiley Online Library for rules of use; OA articles are governed by the applicable Creative Commons License

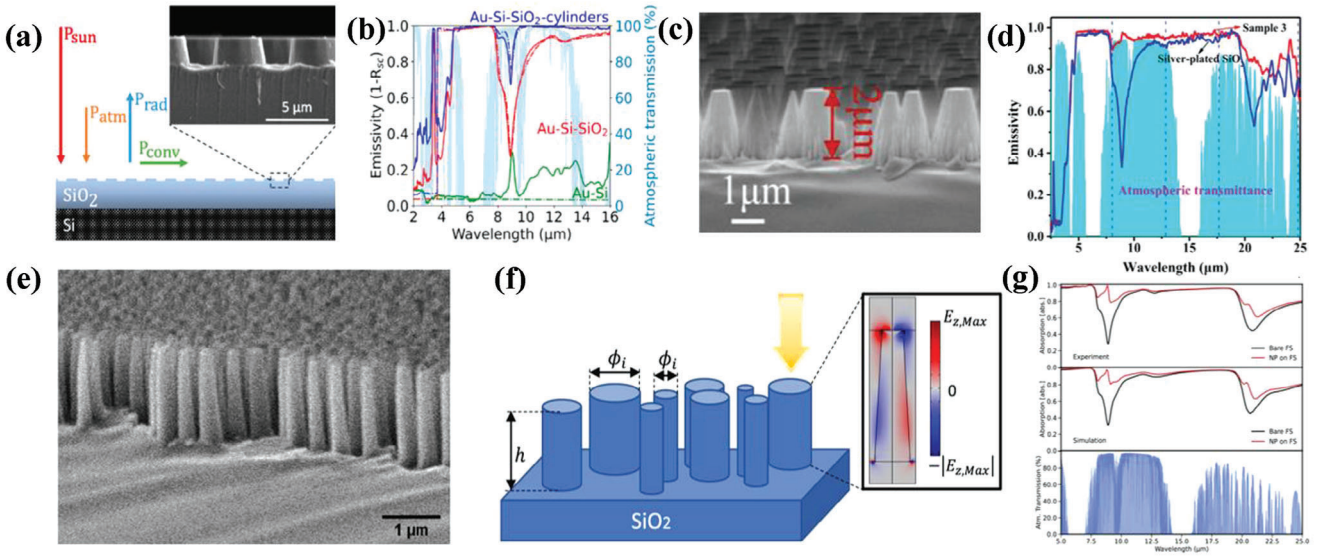


Figure 7. Small 2D micropillar thermal emitter design. a) Schematic diagram of the radiative cooler and basic heat transfer process of surface. The inset shows an SEM image of a crosscut of the fabricated microcylinders. b) Measured (solid) and calculated (dashed) IR emissivity of silicon without module glass (green), with flat silica module glass (red), and with microcylinder module glass (blue). Reproduced with permission.[39] Copyright 2022, American Chemical Society. c) SEM images of the fabricated sample. d) Measured emissivity in the mid-to-long infrared wavelengths from 2.5 to 25 μm, together with the atmospheric transmittance. Reproduced with permission.[37] Copyright 2022, Wiley-VCH. e) SEM image of a typical NP surface structure with $h \approx 1250$ nm and $\phi_{\text{Tip-AVG}} = 172$ nm. f) Left: schematics of the proposed surface made of nanopillars (NPs) with height h and average diameter $\phi_{\text{AVG}} = \langle \phi_i \rangle$. Right: simulated electric field distribution in the NP at 9 μm. g) Top panel: experimental optical absorption spectra of flat fused silica (black line) and randomly distributed NPs on fused silica (red line) in the IR optical range. Middle panel: simulated optical absorption spectra. Bottom panel: atmospheric optical transmission in the IR optical range (from 5 to 25 μm). Reproduced with permission.[66] Copyright 2022, American Chemical Society.

which is favorable for the typically unpolarized nature of thermal management applications. The higher uniformity and isotropic arrangement of 2D patterns (especially disordered and/or polydisperse ones) provides also a more gradual refractive index change across the interface, which further enhances the emissivity of the SiO_2 in this band, thus increasing its radiative cooling capacity.

3.5. Microspheres

The procedures utilized for the microstructuring of SiO_2 surfaces are frequently viewed as costly and not readily available for widespread use. Consequently, several researchers have undertaken the use of SiO_2 microspheres to realize both disordered and ordered materials, discussing in detail the additional mechanisms involved in the observed emissivity enhancement. In 2018, Atiganyanun et al.[67] showed that a coating made of densely packed SiO_2 microspheres could increase optical scattering in the solar spectrum and thermal emission in the atmospheric transparency window, surpassing commercially available cooling white paints in terms of daytime cooling. Fan et al.[68] conducted an experiment mixing micro- and nanoscale SiO_2 spheres in different ratios, as schematically represented in **Figure** 8a. The SEM images corresponding to the 1:1 ratio are displayed in Figure 8b, reaching high emissivity within the atmospheric window due to the combined action of both nanoscale and micron-scale SiO_2 particles (Figure 8c). Whitworth et al.[53] provided a comprehensive analysis of the underlying mechanism behind the increased emissivity provided by microspheres, showing that bulk and shell morphologies can serve complementary functions (Figure 8d). SiO_2 micro-shells exhibit an enhanced the emissivity at 8–10 μm through surface phonon polariton excitations (Figure 8e). The 2 μm SiO_2 spheres, on the other hand, can achieve a significant level of radiative coverage in the atmospheric window, as demonstrated in Figure 8f, reaching an average emissivity of 0.65 across a broad range of angles (Figure 8g). Additionally, Jaramillo-Fernandez et al.[40] proposed a cost-effective solution that involves the self-assembly of a single layer of 8 μm diameter silica microspheres on 1 mm thick soda-lime glass (Figure 8h). Figure 8i illustrates how ultra-high IR emissivity is obtained as a combination of three factors. These include the spherical structure of SiO_2, the thermal excitation of surface phonon polaritons (SPhP), and the diffraction of these excitations into the far field through the periodic lattice. The resulting radiative cooler functions as an almost ideal infrared broadband emitter (Figure 8j), so that when it is used to cover a silicon wafer during the daytime, it can reduce its temperature by 14 °C. The use of ordered arrays of SiO_2 microspheres was also investigated by Lin et al.,[69] who developed an all-inorganic narrow-band emitter integrating the microsphere monolayer self-assembled on the surface of a back-silvered SiO_xN_y substrate (Figure 8k). In Figure 8l, the electric fields at the two vibrational peaks of the Si—O bond, i.e., $\lambda = 9.4$ and 12.5 μm, are illustrated, showing that the electric field in the gap between the spheres is magnified by 10 and 6 times, respectively. This amplification contributes to the selective emission enhancement within the atmospheric window of 8–13 μm, resulting in an average emissivity of 0.946 (Figure 8m). Additionally, the tightly arranged monolayers can produce a 20% increase in IR emission compared to randomly distributed SiO_2 spheres of the

© 2023 The Authors. Advanced Materials Interfaces published by Wiley-VCH GmbH

21967350, 2024, 3, Downloaded from https://onlinelibrary.wiley.com/doi/10.1002/admi.202300603 by Istituto Nazionale Di Ricerca Metrologica, Wiley Online Library on [26/01/2024]. See the Terms and Conditions (https://onlinelibrary.wiley.com/terms-and-conditions) on Wiley Online Library for rules of use; OA articles are governed by the applicable Creative Commons License

21967350, 2024, 3, Downloaded from https://onlinelibrary.wiley.com/doi/10.1002/admi.202300603 by Istituto Nazionale Di Ricerca Metrologica, Wiley Online Library on [26/01/2024]. See the Terms and Conditions (https://onlinelibrary.wiley.com/terms-and-conditions) on Wiley Online Library for rules of use; OA articles are governed by the applicable Creative Commons License

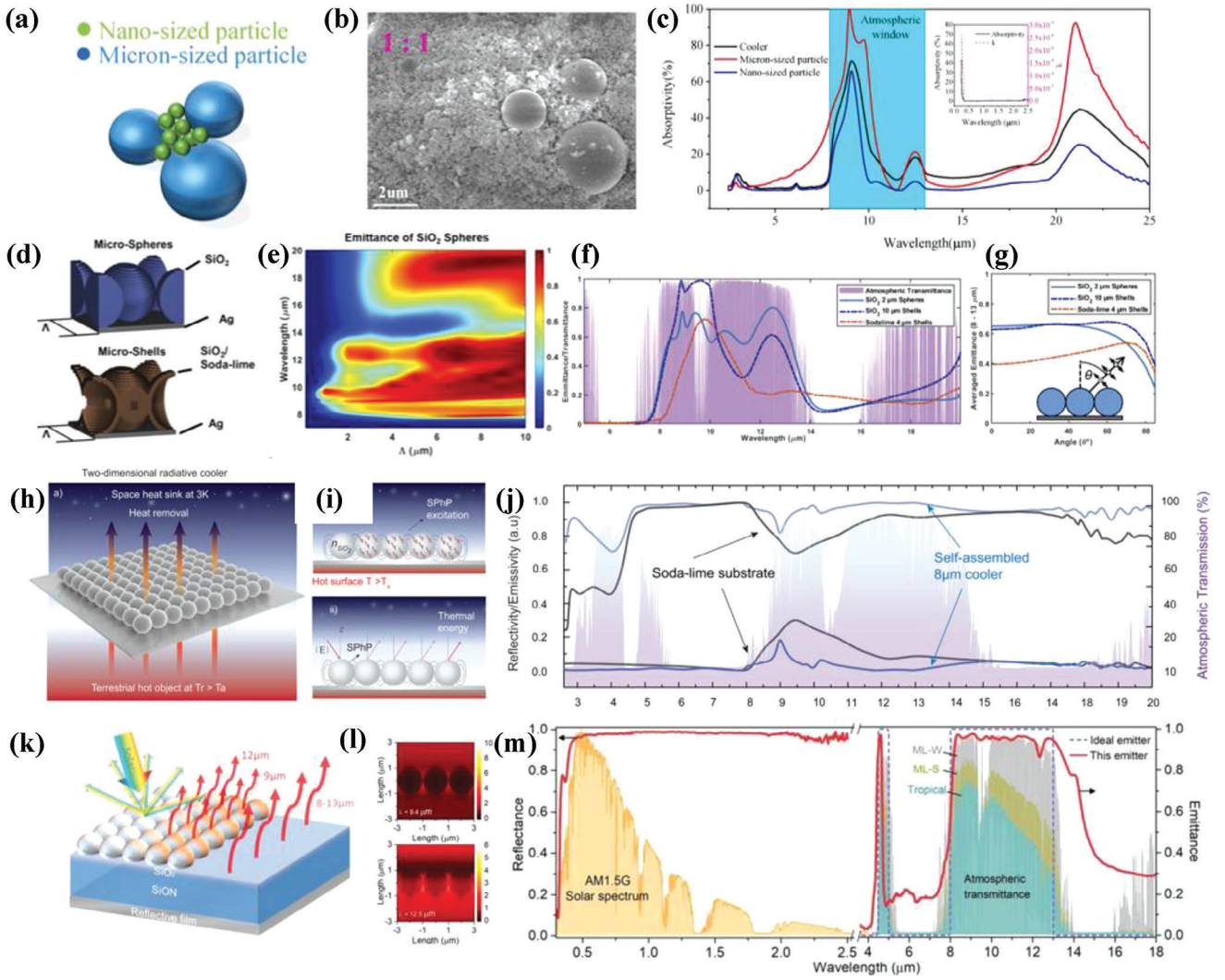


Figure 8. Microsphere-based thermal emitter design. a) Sketch for the packing of micro- and nanoscaled particles. b) SEM images of the radiative coolers with a mixing mass ratio of 1:1. c) Fourier-transform infrared absorption spectrum of the nano-sized particles, micronized particles, and the cooler without PE substrate in the mid-infrared band. Reproduced with permission.[68] Copyright 2020, Elsevier. d) Numerical discretization of the spheres and shells, respectively, used in the rigorous coupled wave analysis calculations. e) The predicted emittance spectra in the IR transparency window are plotted for silica spheres. f) Emittance spectra of the silica spheres, silica shells, and soda-lime shells for sizes which showed the highest value of ΔT for each case: 2, 10, and 4 μm, respectively. The atmospheric transmittance profile is superimposed. g) Average emittance of the three mentioned cases in the atmospheric transparency window (8–13 μm) as a function of angle. Reproduced with permission.[53] Copyright 2021, The Optical Society. h) Schematic representation of the self-assembled 2D radiative cooler. i) Working principle of the 2D radiative cooler. j) Reflectivity and emissivity spectra of soda-lime glass and single-layer radiative cooler made of 8 μm diameter spheres. Reproduced with permission.[40] Copyright 2019, Wiley-VCH. k) Optical structure of the ordered microsphere array emitter. l) Electric field enhancement at 9.4 and 12.5 μm by polariton resonance. m) Solar reflective and thermal emissive spectra of the emitter. Reproduced with permission.[69] Copyright 2022, Wiley-VCH.

same size. Increasing the number of microsphere layers results in the expansion of the emission spectrum, thereby amplifying the potential of this all-inorganic composite film.

4. Summary and Prospects

This review summarized recent research advances in SiO_2 radiative coolers. Currently, constructing 2D micropatterns on the SiO_2 surface represents one of the most effective methods to improve the emissivity of pure SiO_2 in the atmospheric window band (8-13 μm). Based on compatibility and cost-effectiveness considerations, micro pyramids and micropillar structures with a height of up to 2 μm hold promise for a wide range of applications. The intrinsic mechanism behind the atmospheric window emissivity of 2D micropillar-enhanced pure SiO_2 has been thoroughly investigated, with a focus on the involvement of phonon polariton resonance, multipolar modes scattering, and the provision of a gradient equivalent refractive index change. Compared to early attempts, new and highly effective designs have been recently demonstrated which avoid the use of tall and high

© 2023 The Authors. Advanced Materials Interfaces published by Wiley-VCH GmbH

aspect ratio structures, with consequent improvement over the mechanical robustness of the resulting micropatterns. To further decrease the preparation costs associated with radiative coolers and broaden the preparation capacity of SiO_2 radiative coolers, extensive research has been undertaken regarding the infrared thermal radiative characteristics of SiO_2 microspheres. Selective or broadband highly-emissive radiative coolers can be achieved through the self-assembly of microspheres of specific sizes and can be readily scaled up using Langmuir–Schaefer self-assembly technology. In this case, the atmospheric window emissivity of SiO_2 can be modulated by three primary factors: the spherical structure of SiO_2, the thermal excitation of surface phonon polaritons (SPhP), and the diffraction of these excitations through the periodic lattice to the far field. Nonetheless, the mechanical adhesion of the microspheres to the substrate should still be properly addressed for practical applications. To this end, Zhang et al.[73] recently proposed to stabilize these particles into an organic binder, which however introduces again the typical disadvantages associated to the presence of polymeric components compared to fully inorganic and monolithic solutions.

The exceptional stability of SiO_2 radiative coolers renders them ideal candidates for use in all sky-facing equipment and applications that already involve a protective layer of SiO_2. By adopting this approach, the service life of these devices can be significantly extended, ultimately leading to a reduction in operating costs. Such a development is critical for the timely implementation and adoption of SiO_2 radiative cooling devices in the market. On the other hand, it is foreseeable that the utilization of numerical simulation methods complemented with current gradient-based adjoint optimization methods will provide further insights into optimal structural parameters and morphologies, potentially adding further functionalities such as structural coloration. The high stability, low cost, and non-toxicity of SiO_2 radiative cooling materials, combined with the possibility to engineer its emissivity, make it a prominent choice for durable and standardized passive radiative cooling applications. Interesting prospects are envisioned especially in the photovoltaic field, which is typically characterized by above-ambient operating temperatures that are extremely suitable for strong and broadband radiative emitters. Oelker et al.[74] recently explored this idea by proposing a soda lime glass photonic microsphere-based array as an all-photonic radiative cooling approach for improved thermal management of solar cells. In this all-photonic approach related to photovoltaic systems,[38–40,45,61,62,65] the objective is to maximize the broad-band thermal emittance in the infrared range while optimizing light reflection in wavelength ranges where photons are not converted into photocurrent. These characteristics minimize heat gain due to inefficient light-electricity conversion while providing radiative cooling. Overall, these investigations suggest the promising potential of SiO_2-based materials for practical applications in the field of solar energy and for the passive thermal management of solar cells, thereby paving the way for their real-world implementation in the photovoltaic industry.

Not least, SiO_2 or glass materials used for outdoor applications must consider their anti-fog performance and self-cleaning capabilities. Oh et al.[75] developed a composite film of deep sub-wavelength scale colloidal silica nanoparticles and chain-shaped gas-phase silica nanoparticles, which can provide fog-free anti-reflection in the visible wavelength range (380-780 nm) and self-cleaning abilities. Similarly, Rombaut et al.[72] demonstrated that the modification of SiO_2 microcone structures with fluorosilanes can yield anti-reflective films with self-cleaning properties. These results might have relevance for practical applications in the field of solar energy. Remarkable anti-reflection capabilities in the 300–1200 nm spectral band were also reported by Pinto et al.,[76] by adjusting the size of the disordered sub-wavelength structure on the surface of borosilicate glass, and conducting a thorough analysis of the potential applications of these structured glasses in photovoltaic devices. This implies that by altering the structural dimensions of the 2D microcones on the SiO_2 surface and changing its surface, it is possible to expand the functionalities of these SiO_2-like materials, thus leading to a broader range of applications.

Acknowledgements

The authors thank the National Key Research and Development Program of China (2022YFB3902704), the National Natural Science Foundation of China (No.51702068, 52072096), the Natural Science Foundation of Heilongjang Province (LH2023E034) and the Fundamental Research Funds for the Central Universities (HIT OCEF. 2021004). L.P. and J.J.F. acknowledge support from the European project PaRaMetriC, code 21GRD03. The project 21GRD03 PaRaMetriC received funding from the European Partnership on Metrology, co-financed by the European Union's Horizon Europe Research and Innovation Programme, and from the Participating States. Open Access Funding provided by Istituto Nazionale di Ricerca Metrologica within the CRUI-CARE Agreement.

Conflict of Interest

The authors declare no conflict of interest.

Author Contributions

Z.D. and H.L. contributed equally to this work. L.P. and H.X. provided the conceptualization. Y.L. provided the resources and funding acquisition. Z.D. and H.L. initiated the project and wrote the first draft. L.P, J.Z., X.L., H.Z., X.F., J.J.F., and S.N. revised the manuscript. All authors discussed the results and contributed to the writing.

Keywords

photonic design, self-assembly, SiO_2 radiative cooler, structural models

Received: July 12, 2023
Revised: November 3, 2023
Published online: November 27, 2023

[1] D. Zhao, A. Aili, Y. Zhai, S. Xu, G. Tan, X. Yin, R. Yang, *Appl. Phys. Rev.* **2019**, *6*, 021306.
[2] J. Liu, H. Tang, C. Jiang, S. Wu, L. Ye, D. Zhao, Z. Zhou, *Adv. Funct. Mater.* **2022**, *32*, 2206962.
[3] S. Wu, Y. Cao, Y. Li, W. Sun, *Adv. Opt. Mater.* **2022**, *11*, 2202163.
[4] D. Lee, M. Go, S. Son, M. Kim, T. Badloe, H. Lee, J. K. Kim, J. Rho, *Nano Energy* **2021**, *79*, 105426.
[5] B. Zhao, X. Ao, N. Chen, Q. Xuan, M. Hu, G. Pei, *Sol. Energy Mater. Sol. Cells* **2019**, *199*, 108.

© 2023 The Authors. Advanced Materials Interfaces published by Wiley-VCH GmbH

21967350, 2024, 3, Downloaded from https://onlinelibrary.wiley.com/doi/10.1002/admi.202300603 by Istituto Nazionale Di Ricerca Metrologica, Wiley Online Library on [26/01/2024]. See the Terms and Conditions (https://onlinelibrary.wiley.com/terms-and-conditions) on Wiley Online Library for rules of use; OA articles are governed by the applicable Creative Commons License

[6] J. Liu, C. Xu, X. Ao, K. Lu, B. Zhao, G. Pei, *Energy* **2022**, *254*, 124350.
[7] S. Meng, L. Long, Z. Wu, N. Denisuk, Y. Yang, L. Wang, F. Cao, Y. Zhu, *Sol. Energy Mater. Sol. Cells* **2020**, *208*, 110393.
[8] J. Zhang, Z. Zhou, J. Quan, D. Zhang, J. Sui, J. Yu, J. Liu, *Sol. Energy Mater. Sol. Cells* **2021**, *225*, 111029.
[9] R. Xiao, C. Hou, W. Yang, Y. Su, Y. Li, Q. Zhang, P. Gao, H. Wang, *ACS Appl. Mater. Interfaces* **2019**, *11*, 44673.
[10] X. Liu, Y. Li, Y. Pan, Z. Zhou, Z. Zhai, C. Liu, C. Shen, *ACS Appl. Mater. Interfaces* **2023**, *15*, 17188.
[11] J. Li, Y. Fu, J. Zhou, K. Yao, X. Ma, S. Gao, Z. Wang, J.-G. Dai, D. Lei, X. Yu, *Sci. Adv.* **2023**, *9*, eadg1837.
[12] Z. Li, S. Ahmed, T. Ma, *Sol. RRL* **2021**, *5*, 2000735.
[13] K. Gao, H. Shen, Y. Liu, Q. Zhao, Y. Li, J. Liu, *Sol. Energy* **2022**, *236*, 703.
[14] S.-Y. Heo, D. H. Kim, Y. M. Song, G. J. Lee, *Adv. Energy Mater.* **2021**, *12*, 2103258.
[15] D. U. Yildirim, A. Ghobadi, M. C. Soydan, O. Atesal, A. Toprak, M. D. Caliskan, E. Ozbay, *ACS Photonics* **2019**, *6*, 1812.
[16] X. Yin, R. Yang, G. Tan, S. Fan, *Science* **2020**, *370*, 786.
[17] S. Son, Y. Liu, D. Chae, H. Lee, *ACS Appl. Mater. Interfaces* **2020**, *12*, 57832.
[18] Q. Xuan, B. Zhao, C. Wang, L. Li, K. Lu, R. Zhai, X. Liu, B. Jiang, G. Pei, *Energy Convers. Manage.* **2022**, *273*, 116443.
[19] M. Chen, D. Pang, J. Mandal, X. Chen, H. Yan, Y. He, N. Yu, Y. Yang, *Nano Lett.* **2021**, *21*, 1412.
[20] M. Shi, Z. Song, J. Ni, X. Du, Y. Cao, Y. Yang, W. Wang, J. Wang, *ACS Nano* **2023**, *17*, 2029.
[21] B. Xiang, R. Zhang, Y. Luo, S. Zhang, L. Xu, H. Min, S. Tang, X. Meng, *Nano Energy* **2021**, *81*, 105600.
[22] C. Park, C. Park, S. Park, J. Lee, Y. S. Kim, Y. Yoo, *Chem. Eng. J.* **2023**, *459*, 141652.
[23] A. R. Gentle, G. B. Smith, *Nano Lett.* **2010**, *10*, 373.
[24] X. Ji, W. Zha, Q. Luo, G. Li, Y. Du, X. Zhang, *Small* **2023**, *19*, 2301534.
[25] A. P. Raman, M. A. Anoma, L. Zhu, E. Rephaeli, S. Fan, *Nature* **2014**, *515*, 540.
[26] Y. Zhai, Y. Ma, S. N. David, D. Zhao, R. Lou, G. Tan, R. Yang, X. Yin, *Science* **2017**, *355*, 1062.
[27] X. Li, Z. Ding, L. Kong, X. Fan, Y. Li, J. Zhao, L. Pan, D. S. Wiersma, L. Pattelli, H. Xu, *Mater. Adv.* **2023**, *4*, 804.
[28] M.-T. Tsai, S.-W. Chang, Y.-J. Chen, H.-L. Chen, P.-H. Lan, D.-C. Chen, F.-H. Ko, Y.-C. Lo, H.-C. Wang, D. Wan, *Nano Today* **2023**, *48*, 101745.
[29] C. Sonne, B. M. Jenssen, J. Rinklebe, S. S. Lam, M. Hansen, R. Bossi, K. Gustavson, R. Dietz, *Sci. Total Environ.* **2023**, *876*, 162770.
[30] N. D. Tyrrell, *Org. Process Res. Dev.* **2023**, *27*, 1422.
[31] L. Prasittisopin, W. Ferdous, V. Kamchoom, *Dev. Built Environ.* **2023**, *15*, 100188.
[32] T. Wang, Y. Wu, L. Shi, X. Hu, M. Chen, L. Wu, *Nat. Commun.* **2021**, *12*, 365.
[33] S. Jeon, S. Son, S. Y. Lee, D. Chae, J. H. Bae, H. Lee, S J. Oh, *ACS Appl. Mater. Interfaces* **2020**, *12*, 54763.
[34] J. Song, W. Zhang, Z. Sun, M. Pan, F. Tian, X. Li, M. Ye, X. Deng, *Nat. Commun.* **2022**, *13*, 4805.
[35] H. Zhang, K. C. S. Ly, X. Liu, Z. Chen, M. Yan, Z. Wu, X. Wang, Y. Zheng, H. Zhou, T. Fan, *Proc. Natl. Acad. Sci. USA* **2020**, *117*, 14657.
[36] B. Zhao, M. Hu, X. Ao, G. Pei, *Appl. Therm. Eng.* **2019**, *155*, 660.
[37] Z. Ding, L. Pattelli, H. Xu, W. Sun, X. Li, L. Pan, J. Zhao, C. Wang, X. Zhang, Y. Song, J. Qiu, Y. Li, R. Yang, *Small* **2022**, *18*, 2202400.
[38] H. Fathabadi, *IEEE J. Photovoltaics* **2021**, *11*, 1485.
[39] E. Akerboom, T. Veeken, C. Hecker, J. Van De Groep, A. Polman, *ACS Photonics* **2022**, *9*, 3831.
[40] J. Jaramillo-Fernandez, G. L. Whitworth, J. A. Pariente, A. Blanco, P. D. Garcia, C. Lopez, C. M. Sotomayor-Torres, *Small* **2019**, *15*, 1905290.
[41] H. Wang, J. Lin, J. Qi, J. Cao, *J. Mater. Sci. Technol.* **2022**, *108*, 110.
[42] I. H. Malitson, *J. Opt. Soc. Am.* **1965**, *55*, 1205.
[43] M. K. Gunde, *Phys. B-Condens. Matter* **2000**, *292*, 286.
[44] R. Kitamura, L. Pilon, M. Jonasz, *Appl. Opt.* **2007**, *46*, 8118.
[45] L. Zhu, A. Raman, K. X. Wang, M. A. Anoma, S. Fan, *Optica* **2014**, *1*, 32.
[46] J. D. Caldwell, L. Lindsay, V. Giannini, I. Vurgaftman, T. L. Reinecke, S. A. Maier, O. J. Glembocki, *Nanophotonics* **2015**, *4*, 44.
[47] S. Adachi, in *Optical Properties of Crystalline and Amorphous Semiconductors: Materials and Fundamental Principles*, Springer US, Boston, MA **1999**, p. 33.
[48] S. Foteinopoulou, G. C. R. Devarapu, G. S. Subramania, S. Krishna, D. Wasserman, *Nanophotonics* **2019**, *8*, 2129.
[49] J. Kischkat, S. Peters, B. Gruska, M. Semtsiv, M. Chashnikova, M. Klinkmüller, O. Fedosenko, S. Machulik, A. Aleksandrova, G. Monastyrskyi, Y. Flores, W. Ted Masselink, *Appl. Opt.* **2012**, *51*, 6789.
[50] A. Balazadeh Koucheh, M. A. Kecebas, K. Sendur, *J. Quant. Spectrosc. Radiat. Transfer* **2021**, *276*, 107899.
[51] D. Chen, J. Dong, J. Yang, Y. Hua, G. Li, C. Guo, C. Xie, M. Liu, Q. Liu, *Nanoscale* **2018**, *10*, 9450.
[52] C. L. Pinto, I. Cornago, J. Bengoechea, *Energy Technol.* **2023**, *11*, 2300069.
[53] G. L. Whitworth, J. Jaramillo-Fernandez, J. A. Pariente, P. D. Garcia, A. Blanco, C. Lopez, C. M. Sotomayor-Torres, *Opt. Express* **2021**, *29*, 16857.
[54] C. G. Granqvist, A. Hjortsberg, *J. Appl. Phys.* **1981**, *52*, 4205.
[55] Z. Zhang, D. Liu, Z. Xia, J. Chu, J. Shao, presented at 10th Int. Conf. on Thin Film Physics and Applications (TFPA), Qingdao, China, May **2019**.
[56] S. Ishii, T. D. Dao, T. Nagao, *Appl. Phys. Lett.* **2020**, *117*, 013901.
[57] R. A. Yalcin, E. Blandre, K. Joulain, J. Drévillon, *Sol. Energy Mater. Sol. Cells* **2020**, *206*, 110320.
[58] L. Zhu, A. Raman, S. Fan, *Appl. Phys. Lett.* **2013**, *103*, 223902.
[59] E. Blandre, R. A. Yalçin, K. Joulain, J. Drévillon, *Opt. Express* **2020**, *28*, 29703.
[60] Y. Liu, J. Li, C. Liu, *Materials (Basel)* **2021**, *14*, 2637.
[61] B. Zhao, K. Lu, M. Hu, J. Liu, L. Wu, C. Xu, Q. Xuan, G. Pei, *Renewable Energy* **2022**, *191*, 662.
[62] L. Zhu, A. P. Raman, S. Fan, *Proc. Natl. Acad. Sci. USA* **2015**, *112*, 12282.
[63] L. Long, Y. Yang, L. Wang, *Sol. Energy Mater. Sol. Cells* **2019**, *197*, 19.
[64] Y. Li, W. Gao, L. Li, L. Guo, H. Ge, R. Xie, H. Wang, F. Wang, B. An, *Energy Rep.* **2022**, *8*, 852.
[65] Y. Lu, Z. Chen, L. Ai, X. Zhang, J. Zhang, J. Li, W. Wang, R. Tan, N. Dai, W. Song, *Sol. RRL* **2017**, *1*, 1700084.
[66] J. Arres Chillon, B. Paulillo, P. Mazumder, V. Pruneri, *ACS Appl. Nano Mater.* **2022**, *5*, 17606.
[67] S. Atiganyanun, J. B. Plumley, S. J. Han, K. Hsu, J. Cytrynbaum, T. L. Peng, S. M. Han, S. E. Han, *ACS Photonics* **2018**, *5*, 1181.
[68] X. Fan, K. Shi, Z. Xia, *Infrared Phys. Technol.* **2020**, *105*, 103169.
[69] C. Lin, Y. Li, C. Chi, Y. S Kwon, J. Huang, Z. Wu, J. Zheng, G. Liu, C. Y. Tso, C. Y. H. Chao, B. Huang, *Adv. Mater.* **2022**, *34*, 2109350.
[70] M. Chen, D. Pang, X. Chen, H. Yan, *Int. J. Heat Mass Transfer* **2021**, *173*, 121263.
[71] N. J. Ray, J.-H. Yoo, H. T. Nguyen, E. Feigenbaum, *J. Phys.: Photonics* **2021**, *3*, 032004.
[72] J. Rombaut, S. Martínez, U. M. Matera, P. Mazumder, V. Pruneri, *ACS Photonics* **2021**, *8*, 894.
[73] M. Chen, D. Pang, H. Yan, *Appl. Therm. Eng.* **2022**, *216*, 119125.
[74] G. Silva-Oelker, J. Jaramillo-Fernandez, *Opt. Express* **2022**, *30*, 32965.
[75] S. Oh, J.-W. Cho, J. Lee, J. Han, S.-K. Kim, Y. Nam, *Adv. Sci. (Weinh)* **2022**, *9*, 2202781.
[76] C. L. Pinto, I. Cornago, A. Buceta, E. Zugasti, J. Bengoechea, *Sol. Energy Mater. Sol. Cells* **2022**, *246*, 111935.

© 2023 The Authors. Advanced Materials Interfaces published by Wiley-VCH GmbH

21967350, 2024, 3, Downloaded from https://onlinelibrary.wiley.com/doi/10.1002/admi.202300603 by Istituto Nazionale Di Ricerca Metrologica, Wiley Online Library on [26/01/2024]. See the Terms and Conditions (https://onlinelibrary.wiley.com/terms-and-conditions) on Wiley Online Library for rules of use; OA articles are governed by the applicable Creative Commons License



Zhenmin Ding has been studying under the supervision of Prof. Hongbo Xu and Prof. Ying Song since 2020 and is pursuing his Ph.D. degree in engineering at Harbin Institute of Technology, China. His research focuses on analyzing the SiO_2-based infrared emission modulation mechanism and its potential for radiative cooling applications.



Honglin Li is currently pursuing her master's degree at the School of Chemistry and Chemical Engineering, Harbin Institute of Technology. Her research interests focus mainly on the design, fabrication and application of MOFs polymer-based radiative cooling materials.



Juliana Jaramillo Fernandez is a tenure track professor at Universitat Politècnica de Catalunya, specialized in Thermal Nanoscience and Engineering for sustainable thermal management. She is a partner leading researcher of the PATHFINDER project ADAPTATION working on combining energy harvesting and temperature regulation, and contributor to the European Metrology Partnership 21GRD03 PaRaMetriC on the standardization of radiative cooling materials.



Lorenzo Pattelli is a researcher at the Istituto Nazionale di Ricerca Metrologica (INRiM) in Italy. His main research interests include the design, characterization and modeling of scattering media, disordered photonics applications, and bio-inspired materials. He is currently coordinating the European Metrology Partnership 21GRD03 PaRaMetriC on the standardization of passive radiative cooling materials.

© 2023 The Authors. Advanced Materials Interfaces published by Wiley-VCH GmbH

21967350, 2024, 3, Downloaded from https://onlinelibrary.wiley.com/doi/10.1002/admi.202300603 by Istituto Nazionale Di Ricerca Metrologica, Wiley Online Library on [26/01/2024]. See the Terms and Conditions (https://onlinelibrary.wiley.com/terms-and-conditions) on Wiley Online Library for rules of use; OA articles are governed by the applicable Creative Commons License



Yao Li has been a professor of materials science at Harbin Institute of Technology (HIT) since 2005 and leads the Laboratory of Functional Composite Materials in the Center for Composite Materials and Structure. His research interests include fabrication and engineering of chromic materials and their applications for optical and thermal regulation.



Hongbo Xu is currently an associate professor in the School of Chemistry and Chemical Engineering, Harbin Institute of Technology. He received his Ph.D. degree (2011) from the College of Chemistry, Jilin University. His current research focuses on biomimetic optical and thermal materials with micro/nanoscale hierarchical structures, optical surfaces in nature, and biomimetic optical device design and fabrication.

© 2023 The Authors. Advanced Materials Interfaces published by Wiley-VCH GmbH

21967350, 2024, 3, Downloaded from https://onlinelibrary.wiley.com/doi/10.1002/admi.202300603 by Istituto Nazionale Di Ricerca Metrologica, Wiley Online Library on [26/01/2024]. See the Terms and Conditions (https://onlinelibrary.wiley.com/terms-and-conditions) on Wiley Online Library for rules of use; OA articles are governed by the applicable Creative Commons License